Selective Recording of the Canine Hypoglossal Nerve Using a Multicontact Flat Interface Nerve Electrode

Paul B. Yoo, *Member, IEEE,* and Dominique M. Durand*, *Member, IEEE*

***Abstract*—A flat-interface nerve electrode (FINE) is presented as a potential solution for using multifascicle nerve recordings as part of a closed-loop control system. To investigate the ability of this electrode to achieve selective recordings at physiological signal-to-noise ratio (SNR), a finite-element model (FEM) of a beagle hypoglossal nerve with an implanted FINE was constructed. Action potentials (AP) were generated at various SNR levels and the performance of the electrode was assessed with a selectivity index ($0 \leq \mathrm{SI} \leq 1$; ability of the electrode to distinguish two active sources). Computer simulations yielded a selective range ($0.05 \leq \mathrm{SI} \leq 0.76$) that was 1) related to the interfiber distance and 2) used to predict the minimum interfiber distance ($0.23\ \mathrm{mm} \leq d \leq 1.42\ \mathrm{mm}$) for selective recording at each SNR. The SI was further evaluated using recorded compound APs elicited from electrically activating the branches of the beagle hypoglossal nerve. For all experiments ($n = 7$), the selectivity ($\mathrm{SI} = 0.45 \pm 0.16$) was within the range predicted by the FEM. This study suggests that the FINE can record the activity from a multifasciculated nerve and, more importantly, distinguish neural signals from pairs of fascicles at physiologic SNR.**

***Index Terms*—Action potential (AP), beagle hypoglossal nerve, cuff electrode, neural recording, selectivity index, signal-to-noise ratio (SNR).**

I. Introduction

THE therapeutic significance of functional electrical stimulation (FES) is underscored by the myriad of neuroprosthetic devices that have been applied to physiologically impaired organs or systems. For these implantable prostheses, the design criteria are chosen to influence the nervous system at specific levels (i.e., peripheral or central) and for various applications: bladder control [1], [2], functional reanimation of the upper and lower extremities [3]–[6], auditory and visual restoration [7]–[9], respiratory disorders [10], [11], and treatment of Parkinson's disease [12]. Equally important to the *efferent* effects of these implementations, however, is the ability to detect the functional and/or dysfunctional state of the biological system and to use this information to control (i.e., initiate, modulate and terminate) stimulation.

In contrast to conventional artificial sensors (e.g., joint angle transducer), which exhibit problems such as maintenance, cosmesis and biocompatibility, direct recording of electrical activity from biological sources has proven to be an effective means of acquiring reliable control signals. These generally include electromyographic (EMG) and electroneurographic (ENG) recordings obtained from implanted wire or surface muscle electrodes and nerve cuff electrodes, respectively [13], [14]. More recently, the development of multicontact electrode arrays fabricated at the micron level have initiated novel methods for obtaining cortical signals, which may particularly benefit FES systems involving individuals with spinal cord injury (SCI) at high cervical levels. This approach is commonly referred to as the brain-computer interface (BCI) and involves electrical recordings derived from higher neural structures: electroencephalogram (EEG) and more invasive recordings from various cortical areas [15]–[17].

For most individuals with SCI and stroke survivors, a significant portion of the peripheral nervous system is intact and can provide viable sources for FES control signals. As such, recording the electrical activity from a whole nerve or functionally specific branches is a particularly appealing choice. Unlike recording methods associated with EMG or EEG, direct neural recordings are specific and provide rapid feedback. In addition to the relatively noninvasive surgical procedure associated with nerve cuff electrodes, the reported long-term reliability and safety of these devices offer further validation for the implementation of this technology into FES systems [18]–[20]. The majority of FES applications, however, involve nerve trunks (e.g., radial, sciatic or hypoglossal nerves) that consist of multiple bundles of motor and sensory fibers, the electrical activity of which could be used to control both the *afferent* and *efferent* pathways involved with the prosthesis. As a consequence, multicontact cuff electrodes have been developed to circumvent the need for multiple electrodes implanted on each distal nerve branch. While numerous studies have documented the selective stimulation properties of these conventionally round (i.e., transverse geometry) and even self-sizing electrodes [21], [22], there is a paucity of experimental data concerning the ability of such electrodes to record and distinguish between different active fascicles [23], [24].

The flat-interface nerve electrode (FINE) presents a unique cuff electrode design for selective nerve recording by realigning the fascicles and reshaping the nerve into a more flattened cross section [25]. This anatomical modification increases the surface area of the exposed nerve and, in turn, offers greater access to fascicles, which may otherwise be surrounded by adjacent fascicles. Improvements in the recording characteristics of this electrode (compared to round transverse geometry) have been demonstrated in a previous modeling study for geometrically idealized neuroanatomical structures [26].

Manuscript received April 14, 2004; revised August 29, 2004. This work was supported by the National Institutes of Health, NINDS Grant 1 R01 HL66267-01. *Asterisk indicates corresponding author.*

P. B. Yoo was with the Neural Engineering Center of the Biomedical Engineering Department, Case Western Reserve University, Cleveland, OH 44106 USA. He is now with the Biomedical Engineering Department, Duke University, Durham, NC 27708 USA (e-mail: pby2@duke.edu).

*D. M. Durand is with the Neural Engineering Center of the Biomedical Engineering Department, Case Western Reserve University, Cleveland, OH 44106 USA (e-mail: dxd6@case.edu).

Digital Object Identifier 10.1109/TBME.2005.851482

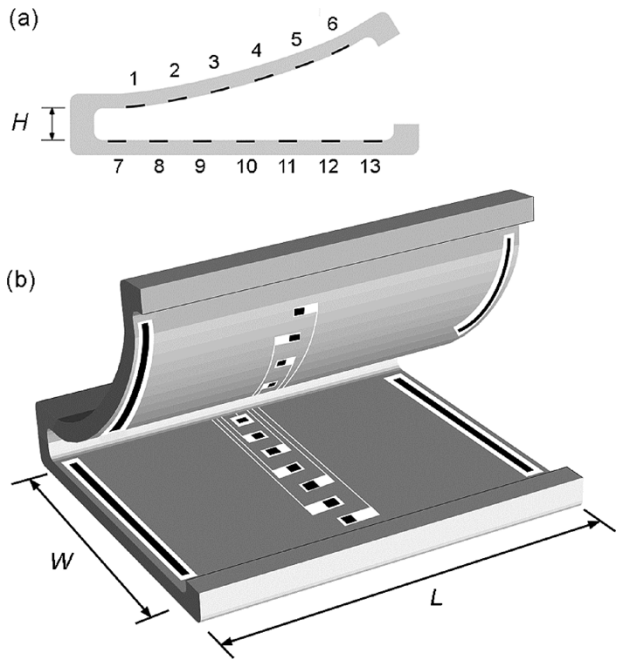

Fig. 1. Schematic diagram of the FINE. (a) Cross section of the FINE with all thirteen recording positions (i.e., cathodes) and height of electrode opening labeled 1–13 and H, respectively. (b) Rotated drawing of the FINE showing the spot-welded platinum pieces (white) and the exposed cathodic (0.5 mm × 0.5 mm) and anodic contacts (black; 0.5 mm × 6.5 mm). Tripolar recording is achieved by measuring the differential voltage between the center cathode and the electrically shorted anodes. The width (W) and length (L) of the space inside the FINE are labeled accordingly.

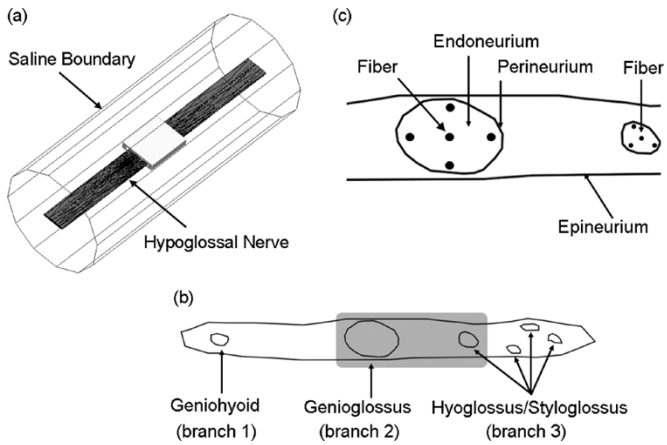

Fig. 2. FEM of a cuff electrode and hypoglossal nerve. The solved model is depicted by the surface mesh. (a) The active voltage source is located just outside the FINE and immersed in a cylindrical volume of saline. (b) Image of the nerve cross section with the fascicles (GH; GG; and HG/SG) and functional branches (branches 1–3) labeled. (c) Zoomed image of the shaded area in (b), where the typical locations of nerve fibers are denoted by the dots. Five evenly spaced fibers were placed in the fascicles corresponding to the GH and GG, while only four axons were placed in the fascicles innervating the HG/SG (i.e., $\mathrm{total} = 26$).

TABLE I
ELECTRICAL PROPERTIES OF PERIPHERAL NERVE

Material	Conductivity (S/m)	Reference
Endoneurium	8.26e-2 (transverse)	[42-44]
	5.71e-1(longitudinal)	[42-44]
Perineurium	2.1e-3	[42]
Epineurium	8.26e-2	[42]
Silicone	1e-7	[26]
Saline	2	[26,43]

This paper examines the feasibility of selectively recording the neural activity of a multifasciculated nerve using the FINE. First, a three dimensional finite-element model (FEM) was derived from a cross-sectional image of a canine hypoglossal nerve. The model could generate single fiber action potential (AP) signals to: 1) investigate the recording selectivity (i.e., ability to distinguish two active fascicles) at various signal-to-noise ratio (SNR) levels and 2) determine the optimum number of electrode recording positions. The model was validated subsequently via acute beagle experiments: hypoglossal nerve branches were electrically stimulated, while compound APs were recorded with the FINE and used to quantify the performance of the electrode. Preliminary results of this study have been previously reported [27].

II. METHOD

The recording selectivity of the FINE was investigated using both computational and experimental approaches. In both cases, the electrical activity of the canine hypoglossal nerve was recorded with a multicontact FINE [Fig. 1(a)] to quantify electrode performance. All animal care and experimental protocols were in accordance with NIH guidelines and approved by the Institutional Animal Care and Use Committee of Case Western Reserve University.

A. FEM

A cross section of the canine hypoglossal nerve corresponding to the location at the cathodes of a FINE was traced, digitized and translated into a finite element software package (Maxwell 3D, Ansoft Corp.). The electrically anisotropic endoneurium, epineurium, and perineurium $(\mathrm{thickness} = 50\ \mu\mathrm{m})$ were extruded [$\mathrm{length} = 60$ mm; Fig. 2(a)–(c)] and enclosed within a silastic cuff representing the FINE [$L \times W \times H = 1\ \mathrm{cm} \times 6.5\ \mathrm{cm} \times 0.5$ mm; Fig. 1(b)]. The electrical conductivity of each model component is presented in Table I. A single cylindrical voltage source (node of Ranvier at 0.1 V; $\mathrm{radius} = 3\ \mu\mathrm{m}$; $\mathrm{length} = 4\ \mu\mathrm{m}$) was placed within one of the fascicles to represent a node of Ranvier, while the outer boundary of the cylindrical volume of saline ($\mathrm{radius} = 12$ mm; $\mathrm{length} = 60$ mm) was defined as the electrical ground [Fig. 1(a)]. A simple analysis of the model [results not shown] determined that the accuracy of the FEM solution was unaffected for dimensions of saline that were two orders of magnitude greater than the source.

In order to account for the contribution of each node of Ranvier along the nerve to the recorded electric potential within the FINE, the FEM was repeatedly solved (computation time >15 min per node of Ranvier; number of elements (tetrahedra) >60 000) as the voltage source was displaced at 1 mm intervals, as depicted in Fig. 3(a). Each solution of the model yielded 1) the electric potential at the anodic and cathodic recording positions within the FINE and 2) the total current exiting the voltage source that was defined as the *nodal current* (I_{ANSOFT}). This series of computations was repeated for various locations of the nerve fiber within any one of the fascicles [Fig. 2(c)].

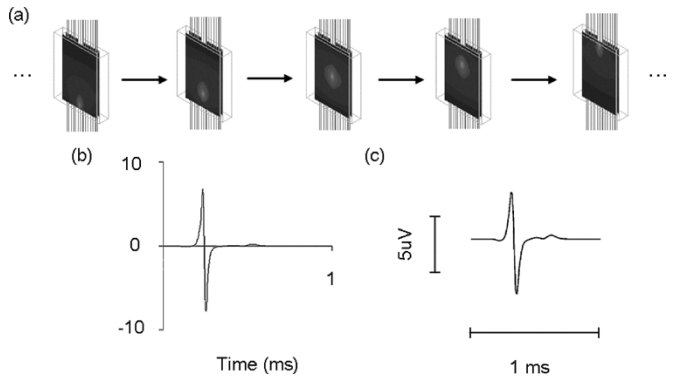

Fig. 3. Single fiber action potential. (a) Sequential images of the solved electrical field potential on the inner surface of the cuff electrode as the node of Ranvier is displaced along the nerve. In this example, the interval distance is 0.5 mm. (b) Time-dependent nodal current (I_{NEURON}) obtained from a myelinated axon model (NEURON) using mammalian membrane dynamics (Sweeney *et al.*, 1987). (c) An example of a computationally generated single fiber action potential.

B. Computational Simulation of Action Potentials

A computational algorithm (Matlab, Mathworks Inc.) was created to simulate action potential recordings from a single active 10-μm fiber. At each microsecond, the number of active nodes of Ranvier was determined according to the saltatory conduction properties of a propagating action potential [30]. Based on a NEURON computer model ([28]) of a myelinated mammalian axon activated via intracellular current injection [29], the membrane current of a single node of Ranvier [I_{NEURON} in Fig. 3(b)] was then obtained and used to linearly scale (I_{NEURON}: I_{ANSOFT}) the electric potential corresponding to each active node of Ranvier. The final tripolar nerve cuff recordings [$\mathrm{V_{tripole}(t) = V_{cathode}(t) - V_{anode}(t)}$; Fig. 3(c)] were generated by summing these scaled voltages at each time interval. It is noted that while the number of recording contacts on the FINE used in the animal experiments was thirteen, the FEM employed a greater number of recording positions ($\mathrm{n = 26}$) to explore the limits of the FINE. These are shown in Figs. 6(a) and 7(a), respectively.

C. Acute Canine Experiments

Six adult beagles (9–12 kg) were anesthetized with an initial I.V. injection of 2.5% sodium thiopental (1 ml/kg) and subsequent ventilation of 1%–3% halothane with 100% oxygen. With the dog placed in a supine position (Fig. 4) an incision along the submandibular region (i.e., hyoid bone to mandible) and blunt dissection of the underlying fascia and muscle tissue were performed to expose the hypoglossal nerve and its distal branches. A multicontact FINE (Fig. 1) was implanted just proximal to the branching point of the hypoglossal nerve, while single tripole FINEs were placed on each accessible distal nerve branch. While the branches innervating the GH and GG muscles usually consisted of a single fascicle, the nerve branch associated with the tongue retractors (HG and SG) contained multiple fascicles that formed an aggregate of small branches. Consequently, these functionally homologous branches were grouped into a single electrode.

As the individual hypoglossal nerve branches of each beagle ($n = 7$) were maximally activated by current pulses

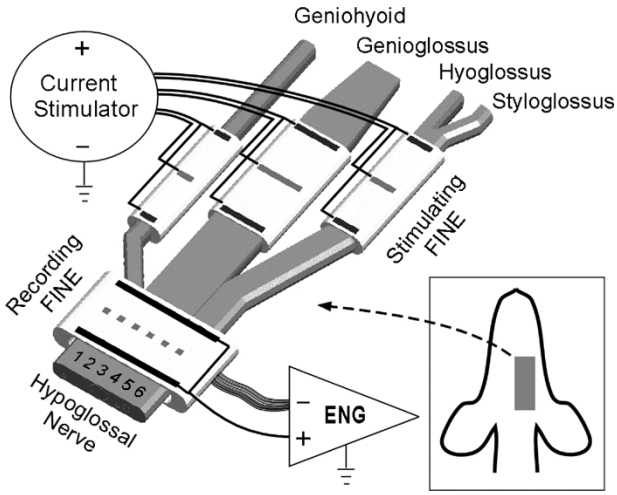

Fig. 4. Schematic of acute beagle experiment. Current pulses were delivered through one of the stimulating FINEs implanted on each nerve branch, while compound APs were filtered, amplified (differential amplifier) and recorded with the recording FINE. Note the anodes of the FINE are electrically shorted in the conventional tripolar configuration. The innervated muscles and corresponding nerve branches are labeled, accordingly. The site of submandibular incision in the beagle is indicated as the shaded area in the inset.

($I = 0.5$ to 2 mA; pulse width $= 50\ \mu$s; $f = 2$ Hz; $n = 16$) delivered through the corresponding single-tripole FINE, antidromic compound action potentials (CAP) were recorded using a 13-tripole FINE (Fig. 4). The recorded signals were filtered (bandpass: 10 Hz–10 kHz; notch: 60 Hz) and amplified (gain: 5000–100 000) with an ac-coupled differential amplifier (Grass P511, Astromed Inc.) and digitally archived ($\mathrm{sampling\ rate = 40\ kHz}$).

Prior to euthanasia, the nerve was severed distal and proximal to the stimulating and recording electrodes, respectively. The hypoglossal nerve and recording FINE were stored in 10% formalin solution. The nerve was later sectioned into 1-cm segments, embedded in paraffin, sliced, and stained with methylene blue to yield cross-sectional images of the nerve.

D. Selectivity Index

The performance of the FINE was characterized by a recording selectivity index (SI) and defined as the ability of the electrode to distinguish between two active sources (i.e., anatomical fascicles or functional branches) located within a nerve. The selectivity was quantified by computing the Euclidian distance between two N-dimensional vectors, each generated by two sources and denoted by the peak-to-peak voltage (Vpp) or root-mean-squared (rms) value of the action potentials recorded with the FINE. The amplitude of the evoked neural signal (Vpp) was used to compute SI, unless the selectivity was evaluated for data with finite SNR. In such cases, the rms was used to compute SI. As previously shown [26], these two sets of N-dimensional vectors formed a matrix ($V_{m,n}$) that was normalized to eliminate the effects of electrode contact impedance variability. The recorded signals from each contact ($v_{m,n}$) was divided by the sum of the responses of that contact for all active sources

$$\mathrm{c_{m,n}} = \frac{\mathrm{v_{m,n}}}{\sum_{\mathrm{m=1}}^{2} \mathrm{v_{m,n}}}. \tag{1}$$

Each vector $(c_{m,n})$ was then normalized to unit magnitude to account for the source dependent differences in recorded peak-to-peak amplitudes

$$w_{m,n} = \frac{c_{m,n}}{\sqrt{\left(c_{m,1}^2 + c_{m,2}^2 + \cdots + c_{m,N}^2\right)}}. \quad (2)$$

Following normalization of the matrix, $V_{m,n}$, the Euclidian distance $(0 \leq \mathrm{SI} \leq 1)$ between the vectors defined by the two active sources ($m1$ and $m2$) is calculated as shown in (3) at the bottom of the page.

The lower $(\mathrm{SI} = 0)$ limit of selectivity represents a case where an active fiber yields identical recorded signals at every contact position, while maximum selectivity $(\mathrm{SI} = 1)$ occurs when only one contact is different from the other recording positions (i.e., infinite distance between contacts).

E. Analysis of Nerve Model

To investigate the selective properties of the cuff electrode using a finite-element nerve model, action potential recordings were first generated for active fibers located within each fascicle [Fig. 2(c); $\mathrm{n} = 26$ axons]. The selectivity index for paired sets of these signals was computed for all possible combinations of axons located in different fascicles $(\mathrm{n} = 281)$. Based on the computed SI range for these pairs of active fibers, the effects of nerve geometry (relative position of fascicles within the nerve) on the selectivity were studied via a cluster analysis: 1) fiber pairs were grouped according to interfiber distances that were within $\pm 10\%$ of the mean; 2) each cluster consisted of fiber pairs that were associated with more than one distinct pair of fascicles; and 3) an ANOVA test was used to determine any significant differences within each cluster.

Next, the relationship between the recording selectivity and the electrode contact configuration was investigated. Using single axons located in the middle of active pairs of fascicles, the SI was computed for all possible combinations of n contacts from one (single side; $n = 2$, 3, 5, 7, and 13) or both (double side; $n = 3$, 5, 7, 13, 20, and 26) sides of the nerve electrode [Fig. 7(a)]. The calculated SI for five contacts in the single side case, for example, involved all possible combinations of $n = 5$ contacts chosen from recording positions 1 to 13 in Fig. 7(a). The five contact double-sided SI, on the other hand, was computed by using the combined possibilities of (a) $n = 3$ contacts chosen from recording positions 1 to 13 and (b) $n = 2$ contacts chosen from recording positions 14 to 26.

Finally, to relate the selectivity index to the signal to noise ratio (SNR) of the recorded signals, the nerve model was further analyzed as a function of the amplitude of uniformly distributed random noise added to the computationally generated action potentials. Using the rms value of action potentials recorded with a double-sided 13 contact FINE configuration [see Fig. 5(a)], the SI was calculated for every pair of active fibers $(n = 281)$ at various levels of noise $(0\,\mathrm{dB} \leq \mathrm{SNR} \leq 20\,\mathrm{dB})$.

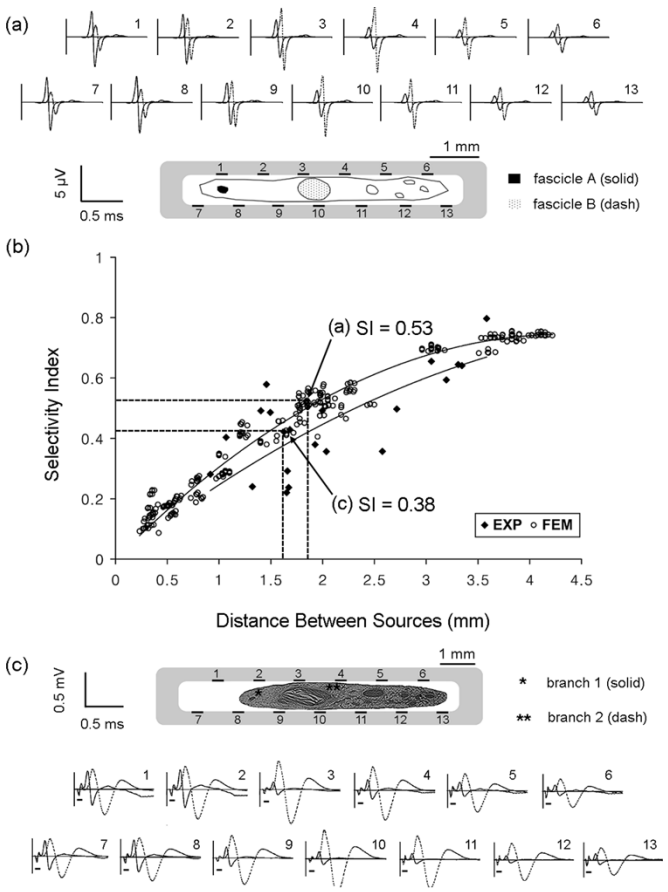

Fig. 5. Sample tripolar recordings obtained from the model (FEM) and experiments (EXP) are shown in (a) and (c), respectively. The paired signals (solid and dashed lines) are numbered according to the contact position. (b) The selectivity was subsequently computed for all combinations of fibers (FEM: $\mathrm{n} = 281$) and fascicles (EXP: $\mathrm{n} = 21$) and plotted as a function of the distance between the two sources. The SI for the signals in (a) and (c) are indicated by the arrows: $\mathrm{SI} = 0.53$ at 1.85 mm and $\mathrm{SI} = 0.38$ at 1.53 mm, respectively. The data were fitted second-order polynomials: (a) $\mathrm{y} = -0.04\mathrm{x}^2 + 0.34\mathrm{x}$ $(\mathrm{r}^2 = 0.97)$; (b) $\mathrm{y} = -0.03\mathrm{x}^2 + 0.28\mathrm{x}$ $(\mathrm{r}^2 = 0.47)$.

III. Results

A FEM of the canine hypoglossal nerve was used to investigate the recording selectivity of the FINE by computing the SI for pairs of axons located within different fascicles. The computational model was verified through subsequent in vivo experiments $(n = 7)$ that were performed in six beagles. Both the left and right hypoglossal nerves were used in one animal (Exp #6).

A. Recording Selectivity-Simulations

The recording selectivity of a multicontact nerve electrode was studied using a finite element model based on a sample image of a canine hypoglossal nerve. In order to quantify the

$$\mathrm{SI} = \frac{\sqrt{(w_{m1,1} - w_{m2,1})^2 + (w_{m1,2} - w_{m2,2})^2 + \cdots + (w_{m1,N} - w_{m2,N})^2}}{\sqrt{2}}. \quad (3)$$

performance of the electrode, sets of action potential recordings were first simulated for single active axons located within each fascicle [Fig. 2(c)]. For these 10 μm diameter axons and the electrode dimensions used in the model, the exhibited characteristics of the generated action potentials [Fig. 3(c)] were similar to those obtained from Aβ fibers using experimental and computational methods: triphasic waveform, duration and peak-to-peak amplitude [31].

Paired sets of simulated APs corresponding to two active fibers located in different fascicles (denoted as A and B) were used to compute the recording selectivity. An example is shown in Fig. 5(a), where the generated signals for single active fibers located in fascicles A and B were plotted as solid and dashed lines, respectively. The marked difference in the peak-to-peak voltages (V_{pp}) exhibited between contacts located closest (e.g., contact 1) and farthest (e.g., contact 6) from an active fascicle (e.g., fascicle A) predict a high degree of recording selectivity, as indicated by a value of SI $= 0.53$ calculated for the data in Fig. 5(a).

B. Recording Selectivity-In Vivo

The in vivo recording selectivity of the FINE was also investigated. A sample set of data is presented in Fig. 5(c), where sequential activation of branches 1 and 2 resulted in the paired signals labeled according to the number of the recording position. Using the Vpp values of the recorded APs, the SI was computed for all hypoglossal nerve branch combinations and plotted as a function of distance between the middle of each respective branch [Fig. 5(b)]. Similar to the results obtained from the computer model, the FINE exhibited high selectivity values [e.g., SI $= 0.38$ at an interfiber distance of 1.53 mm; Fig. 5(b)] that increased with the measured distance between the electrically activated sources. Furthermore, the second-order polynomial fitted to the data also confirmed the quadratic relationship observed in the model.

C. Effect of Nerve Geometry on Selectivity

Further analysis of the computed SI resulted in five distinct clusters with mean interfiber distances of 0.35, 0.5, 1.8, 2.0, and 3.7 mm, respectively [Fig. 6(b)]. Within each cluster, there were two subsets of fiber pairs that represented different combinations of paired fascicles. For example, as shown in Fig. 6(c), there were a total of 25 fiber pairs corresponding to a mean separation of 2.0 mm. Of these, 13 pairs represented fascicles A and B, while the remaining 12 pairs corresponded to fascicles B and D [Fig. 6(a)]. Given that the position of both the fascicles and axons within the model were randomly determined, a series of ANOVA tests for each cluster revealed that there was no significant difference in the mean SI values between these fascicle pairs. These results indicate that the relative position of the pair of active fibers within the FINE does not significantly affect the recording selectivity.

D. Effect of Electrode Contacts (Number and Configuration) on Selectivity

Using the single- and double-sided electrode configurations previously described, the computed SI (mean $\pm$ standard deviation) was plotted with respect to the number of contacts and

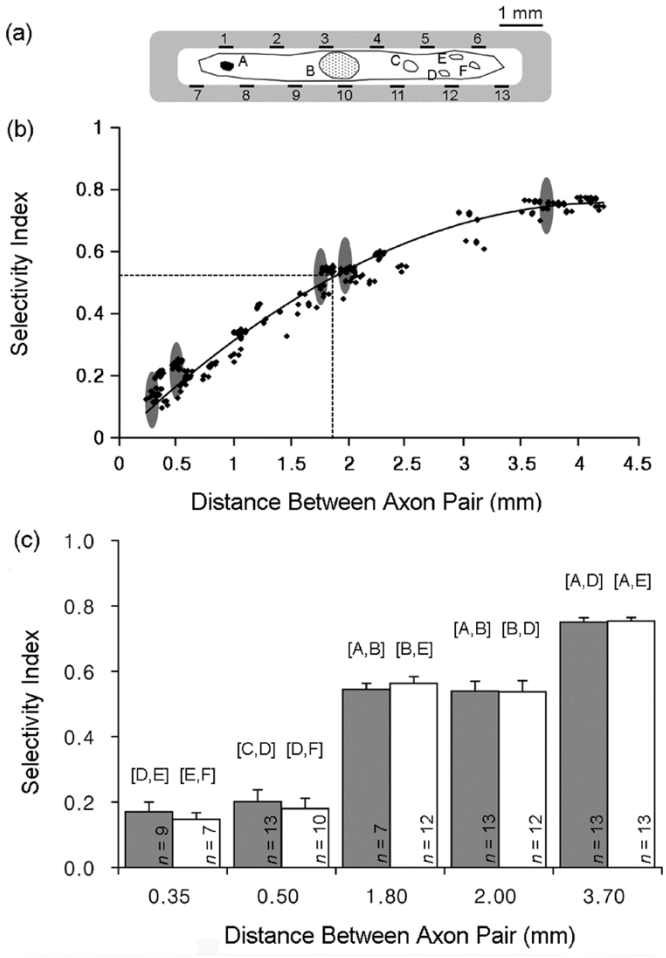

Fig. 6. Analysis of recording SI as a function of nerve geometry. Active fiber pairs were clustered according to two conditions: 1) interfiber distances were within 10% of specified values and 2) each cluster consisted of more than one combination of fascicles. (b) At each specified interfiber distance, paired t-tests were performed between each fascicle combination identified by the letters A-F [refer to image in (a)]. The results show that there was no significant difference in SI between each equidistant pair of fascicles.

shown in Fig. 7(b). The increase and subsequent plateau (at $x = 7$ contacts) for both the single and double-sided SI (e.g., fascicles A and F) were consistently observed for all fascicle combinations of this nerve model. The marked decrease in the standard deviation of SI at $n = 7$ contacts is important, since it represents a threshold beyond which the selectivity is not significantly affected by the number of electrode recording positions. The results of the recording selectivity in Fig. 7(b) (i.e., single versus double at $n = 3$, 5, 7, and 13 contacts) further reveal that there is no significant difference between these electrode recording configurations, regardless of the number of contacts.

Experimental data confirmed these conclusions, where compound action potentials were recorded from canine hypoglossal nerves $(n = 7)$ implanted with a thirteen-contact FINE (Fig. 1). In each experiment, the SI (mean $\pm$ standard deviation) was computed using the recorded peak-to-peak signals from all possible contact combinations for both single ($n = 2$, 3, 5, and 7) and double-sided ($n = 3, 5, 7$, and 13) selectivity. The computed SI values for every branch pair exhibited similar characteristics: 1) the selectivity reached a plateau at $n = 7$ contacts and 2) there was no difference between the single and double-sided contact

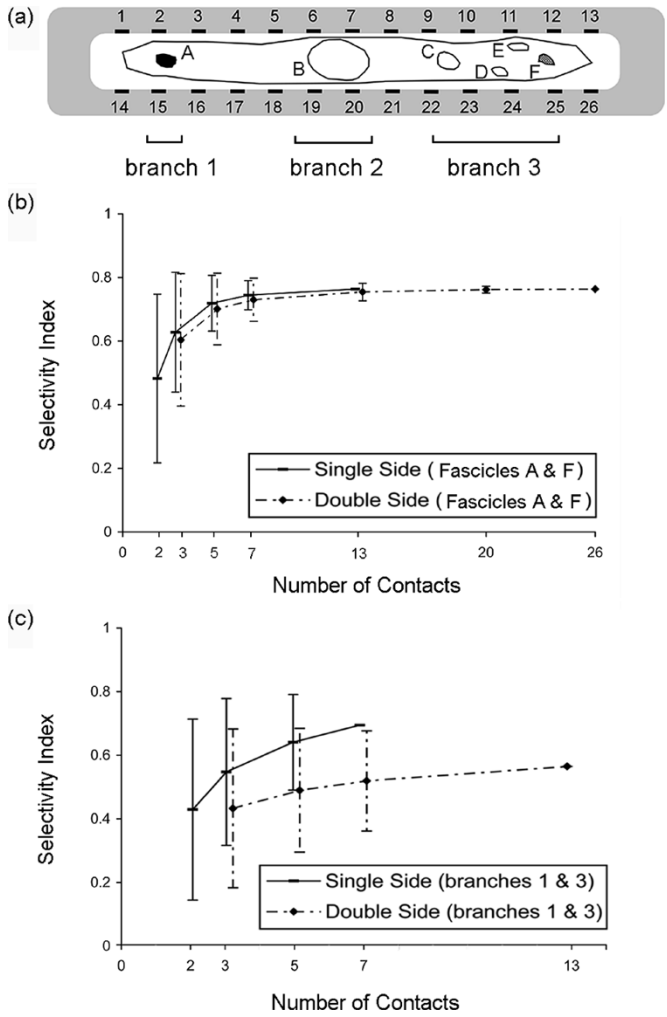

Fig. 7. Effect of the number of recording positions on selectivity. (a) Two active fibers ($\mathrm{interfiber\ distance} = 4.11$ mm) located in the middle of fascicles A and F, respectively, were used to compute SI. (b) The selectivity for this pair was computed for various configurations: all combinations of contacts chosen for one (2, 3, 5, 7, and 13 selected from 13 contacts; solid line) or both sides (3, 5, 7, 13, 20, and 26 selected from 26 contacts; dashed line) of the electrode in (a). The SI increased with the number of electrode contacts and reached a plateau beyond five recording positions. (c) The experimental SI (mean $\pm$ standard deviation, experiment 5) for branches 1 and 3 ($\mathrm{interbranch\ distance} = 3.35$ mm) is plotted as a function of electrode contacts ($x = 2$, 3, 5, 7, and 13) and configuration (single versus double sides). Similar to the nerve model, both configurations reach a plateau at $x = 7$ contacts.

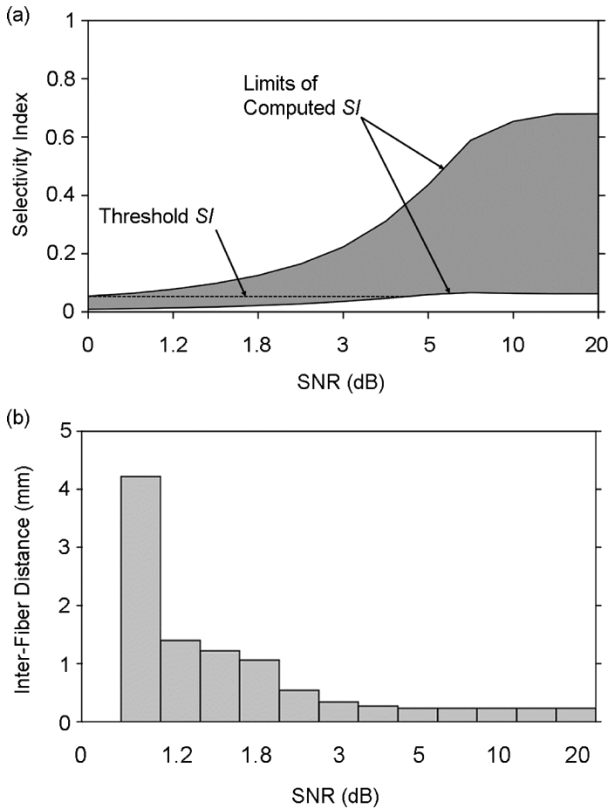

Fig. 8. The effects of random noise on selectivity. As increasingly larger levels of noise was added (i.e., 10 to 100 percent of maximum recorded action potential at 10 percent increments), the SI was re-computed for all possible axon pair combinations ($n = 281$). (a) The upper and lower limits of selectivity are plotted as a function of SNR. The maximum SI ($= 0.05$) at $\mathrm{SNR} = 0$ dB was defined as the threshold SI, below which the pair of recorded signals were equivalent to random noise (i.e., not selective). (b) The threshold SI was used, in turn, to determine the minimum distance between two fibers that could be distinguished (e.g., 0.23 mm for $\mathrm{SNR} \geq 5$ dB).

configurations. The results from one experiment are shown in Fig. 7(c): the single and double-sided SI for branches 1 and 3 are plotted as a function of the number of contacts.

E. Effects of Noise on Selectivity

For this particular analysis of the computer model, the rms values of the generated single fiber action potentials were used to re-compute the selectivity index for all fiber pairs were computed at each noise level. The maximum and minimum SI were respectively defined as the upper and lower limits of the computed SI of each data set and plotted as a function of SNR in Fig. 8(a). The most noticeable characteristic of this plot is that the selective range of the electrode (shaded area) significantly decreases below $\mathrm{SNR} = 5$ dB. In fact, the selective range at $\mathrm{SNR} = 0$ dB is severely limited: $0.01 \leq \mathrm{SI} \leq 0.05$. While any nonzero SI denotes, by definition, a measurable difference in the recorded signals for a given pair of active fibers, the reliability of such an assertion becomes uncertain at $\mathrm{SNR} = 0$ dB as the neural signal is equal to noise. Consequently, the upper limit of selectivity at $\mathrm{SNR} = 0$ dB [$\mathrm{SI} = 0.05$; dashed line in Fig. 8(a)] was defined as the *threshold SI* and represents the minimum selectivity for this model, at which the FINE can distinguish the signal from two fibers. This *threshold SI*, however, further limited the selective range below $\mathrm{SNR} = 5$ dB, as the SI for any fiber pair below 0.05 was not considered selective.

The *threshold SI* was, in turn, used in estimating the minimum possible separation of two selective fibers. At each respective level of SNR, the distance between fiber pairs that yielded the smallest SI greater than the *threshold* was plotted in Fig. 8(b). This minimum distance ranged from the closest pair of fibers (0.23 mm, $\mathrm{SNR} \geq 5$ dB) to the pair corresponding to the largest interfiber distance (4.22 mm, $\mathrm{SNR} \leq 1$ dB) for this nerve model. It is important to note that the FINE [Fig. 8(b)] can selectively distinguish fibers separated by at least 0.54 mm at $\mathrm{SNR} = 2.3$ dB, which is comparable to experimentally observed noise levels [20], [32].

Finally, to test the validity of the computational SI values the experimental SNR was first computed by taking the ratio of the rms value of the maximum recorded compound AP to

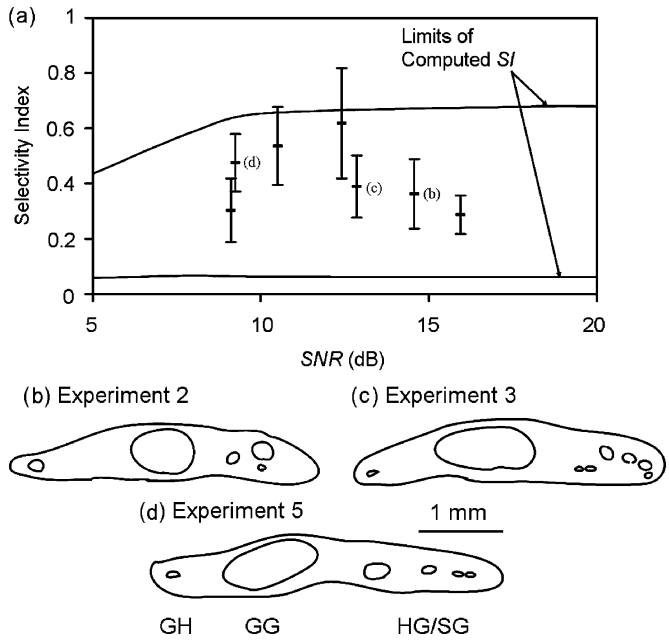

Fig. 9. Experimental selective recording. (a) The experimental SI (mean ± standard deviation) of the FINE was plotted as a function of SNR. The experimental results were within the computed SI limits obtained from the FEM also greater that the *threshold SI*. Traced images of representative canine hypoglossal nerves are indicated in (a) as (b)–(d). The similar SI values are reflected in the nerve cross-sectional geometry of the nerves.

that of the background noise. The recording SI (mean ± standard deviation) were then computed and plotted in Fig. 9(a) as a function of the computed SNR for each respective experiment. The computationally derived upper and lower SI limits of the FEM [refer to Fig. 8(a)] were then superimposed in this plot to directly compare the results. Within the range of experimental SNR, the mean SI values of the FINE were within the predicted limits of the model and were also greater than the minimum (i.e., threshold) selectivity. Furthermore, the predictability of the observed experimental SI is a result of the consistent geometrical properties of the canine hypoglossal nerve, as shown in the traced images in Fig. 9(b), (c).

IV. Discussion

An important design objective for chronically implantable nerve electrodes is to simplify the implementation of the device, which may become particularly critical for applications used, for example, to record the activity of a multifasciculated nerve as part of a feedback control mechanism. To this end, the feasibility of using a single multicontact FINE was investigated. Initially, a FEM was constructed from a digitized image of a canine hypoglossal nerve and used to determine the ability of the electrode to selectively record signals from anatomically separated nerve bundles. The model makes several assumptions to maximize computational efficiency: 1) the generation of neural activity was approximated by a monopolar current source; 2) the anatomical cross section was uniform along the nerve; and 3) linearity allowed scaling and superpositioning voltage recordings from each active node of Ranvier. The observed amplitude, duration and waveform of these simulated single fiber APs were, nevertheless, comparable to those previously reported [26], [31], [33].

The performance of the FINE was quantified with a selectivity index $(0 \leq \mathrm{SI} \leq 1)$ that was defined as the ability of the electrode to distinguish any pair of active sources located within the nerve. Based on a previously derived mathematical expression [26], [34], the SI simply denotes the distance between the end-points of two normalized N-dimensional vectors, which represent the N recording positions of the FINE. This definition ensures that the recording selectivity is not significantly affected by the amplitude of the signal source (e.g., longitudinal position or diameter of fiber). Rather, the SI is determined by the recorded voltage distribution within the cuff electrode, which is strongly related to the interfiber distance, as shown in Fig. 5(b). This relationship is further supported by limited effect of the nerve geometry on the recording selectivity of the FINE. As shown in Fig. 6(c), there is no significant difference in the computed SI for equidistant fascicle pairs that occupy different areas of the nerve cross section.

Another factor that influences the selectivity of the FINE is the number of recording positions (i.e., contact density) placed around the nerve. While previous work has shown that maximum overall selectivity is achieved when the number of contacts equals that of the nerve fascicles [26], this generally occurs when the distribution of the contacts are optimally placed with respect to each bundle of fibers. Since the fascicular morphology is assumed to be unknown a priori, our analysis involved computing the SI for all possible contact combinations for each given number of recording positions [Fig. 7(b)]. The results showed that the SI improved with the number of tripoles and reached maximum selectivity at thirteen contacts. In contrast, the experimentally derived SI in Fig. 7(c) shows a significant discrepancy between the two configurations: double-side yielded lower selectivity. This is not only a result of the smaller number of contacts (total 13 positions) used in the experiments, but it is also a function of the relative size of the nerve with respect to the electrode. As shown is Fig. 5(c), the nerve was always smaller than the nerve cuff electrode opening and so there were contacts that were not directly over the nerve. As a consequence, the computed selectivity for such configurations that mainly surrounded the biological saline within the FINE [e.g., contacts 1, 2, 7, 8, and 9 in Fig. 5(c)] yielded poor selectivity and, hence, large variations in SI. The significance of analyzing the electrode contact configuration is underscored by the practical implications of the results: the maximum SI can be approximated with as little as seven recording positions that can be evenly distributed on one or both sides of the FINE [Fig. 7(b), (c)]. This is particularly important in minimizing the complexity of the implanted device while also ensuring selective recording, as the fascicular morphology of the nerve at the site of implantation may not necessarily be predictable nor consistent [35].

It is clear that the upper limit of the recording selectivity for this nerve model $(\mathrm{SI} = 0.76)$ represents a pair of "distinguishable" sources, but this quantity becomes rather ambiguous at the other end of the SI spectrum. As a result, increasingly larger amplitudes of random noise was added to the simulated APs to yield a minimum limit $(thresholdSI = 0.05)$ of selectivity at $\mathrm{SNR} = 0$ dB [Fig. 8(a)]. Given that the signal amplitude is equivalent to the noise at this SNR level, any SI below this threshold was not considered selective. A more significant

outcome of this model was that this noise analysis provided a means of estimating the minimum interfiber distance for "selective" pairs of axons at each respective level of SNR [Fig. 8(b)]. According to the model, the estimated minimum interfiber distances for pairs of axons that can be selectively recorded with the FINE, range from 0.34 to 1.4 mm at typical SNR values observed ($1 \sim 3$ dB) for cuff electrodes [32], [36].

Experimentally, the average recording selectivity of the FINE at each respective SNR [Fig. 9(a)] was within the SI range predicted by the nerve model, thus confirming the results of the FEM. For this series of canine hypoglossal nerves, the cross-sectional images exhibited a consistent pattern at the site of electrode implant, which is reflected in the computed SI values. A large middle fascicle (GG muscle) was found with an adjacent single fascicle innervating the GH and smaller multiple fascicles innervating the HG/SH muscles [Fig. 9(b)]. While it is difficult to predict the performance of the FINE in a chronically implanted application, the average distance between the closest branch pair (i.e., branches 1 and 2; 1.39 $\pm$ 0.37) is sufficiently large enough, according to the nerve model, to achieve selective recording at as low as $\mathrm{SNR} = 1\ \mathrm{dB}$ [$\mathrm{minimum\ interfiber\ distance} = 1.22\ \mathrm{mm}$; Fig. 7(b)].

The recording characteristics of the FINE are achieved through reshaping the nerve and optimizing the spatial orientation of the fascicles, with respect to the contacts of the cuff electrode. This is further enhanced by the inherent noncircular nerve geometry that has been observed near the branching point of peripheral nerves (e.g., hypoglossal or pudendal nerves). The fact that selectivity is improved without compromising the perineurium does not preclude concerns regarding the long-term safety of the FINE [37], [38]. The potentially deleterious effects (e.g., neural damage or functional deficit) of neural reshaping are justifiably anticipated by the observed sequelae of compression forces on peripheral nerves [39], [40]. Nevertheless, these issues may be circumvented by avoiding severe fascicular reshaping as recently shown in the rodent sciatic nerve: the FINE reshaped the nerve without causing significant postimplant changes in nerve histology or physiology [41].

This paper presents several important findings: 1) the recording selectivity of the FINE is dependent on the distance between the active sources; 2) the number of recording positions (i.e., contact density) influences the recording SI; and 3) a FEM can be used to estimate the minimum interfiber distance that can be selectively recorded with the FINE. While the model suggests that the FINE could selectively record sources at physiological SNR levels ($1 \sim 3$ dB) that are separated by as little as 340 μm, the evoked compound action potentials of the experimental data limit the predictions of the model. Further studies involving naturally generated neural activity (i.e., $\mathrm{SNR} < 3\ \mathrm{dB}$) and signal extraction algorithms such as blind source separation should yield greater insight into the limits of selective nerve recording.

ACKNOWLEDGMENT

The authors would like to thank K. Leder and K. J. Gustafson for their help with experiments, and also P. Parikh for helping with the computer simulations.

REFERENCES

[1] W. M. Grill, N. Bhadra, and B. Wang, "Bladder and urethral pressures evoked by microstimulation of the sacral spinal cord in cats," *Brain Res.*, vol. 836, pp. 19–30, 1999.

[2] G. S. Brindley, "Emptying the bladder by stimulating sacral ventral roots," *J. Physiol.*, vol. 237, pp. 15P–16P, 1974.

[3] P. Strojnik, R. Acimovic, E. Vavken, V. Simic, and U. Stanic, "Treatment of drop foot using an implantable peroneal underknee stimulator," *Scand. J. Rehabil. Med.*, vol. 19, pp. 37–43, 1987.

[4] P. H. Peckham and G. H. Creasey, "Neural prostheses: clinical applications of functional electrical stimulation in spinal cord injury," *Paraplegia*, vol. 30, pp. 96–101, 1992.

[5] V. K. Mushahwar, D. F. Collins, and A. Prochazka, "Spinal cord microstimulation generates functional limb movements in chronically implanted cats," *Exp. Neurol.*, vol. 163, pp. 422–429, 2000.

[6] P. E. Crago, P. H. Peckham, and G. B. Thrope, "Modulation of muscle force by recruitment during intramuscular stimulation," *IEEE Trans. Biomed. Eng.*, vol. BME-27, pp. 679–684, 1980.

[7] G. M. Clark, Y. C. Tong, R. Black, I. C. Forster, J. F. Patrick, and D. J. Dewhurst, "A multiple electrode cochlear implant," *J. Laryngol. Otol.*, vol. 91, pp. 935–945, 1977.

[8] T. Hillman, A. N. Badi, R. A. Normann, T. Kertesz, and C. Shelton, "Cochlear nerve stimulation with a 3-dimensional penetrating electrode array," *Otol. Neurotol.*, vol. 24, pp. 764–768, 2003.

[9] J. S. Hayes, V. T. Yin, D. Piyathaisere, J. D. Weiland, M. S. Humayun, and G. Dagnelie, "Visually guided performance of simple tasks using simulated prosthetic vision," *Artif. Organs*, vol. 27, pp. 1016–1028, 2003.

[10] A. F. DiMarco, R. P. Onders, K. E. Kowalski, M. E. Miller, S. Ferek, and J. T. Mortimer, "Phrenic nerve pacing in a tetraplegic patient via intramuscular diaphragm electrodes," *Am. J. Respir. Crit. Care Med.*, vol. 166, pp. 1604–1606, 2002.

[11] A. Oliven, D. J. O'Hearn, A. Boudewyns, M. Odeh, W. De Backer, P. van de Heyning, P. L. Smith, D. W. Eisele, L. Allan, H. Schneider, R. Testerman, and A. R. Schwartz, "Upper airway response to electrical stimulation of the genioglossus in obstructive sleep apnea," *J. Appl. Physiol.*, vol. 95, pp. 2023–2029, 2003.

[12] A. L. Benabid, A. Koudsie, A. Benazzouz, V. Fraix, A. Ashraf, J. F. Le Bas, S. Chabardes, and P. Pollak, "Subthalamic stimulation for Parkinson's disease," *Arch. Med. Res.*, vol. 31, pp. 282–289, 2000.

[13] K. D. Strange and J. A. Hoffer, "Gait phase information provided by sensory nerve activity during walking: applicability as state controller feedback for FES," *IEEE Trans. Biomed. Eng.*, vol. 46, no. 7, pp. 797–809, Jul. 1999.

[14] D. B. Popovic, R. B. Stein, K. L. Jovanovic, R. Dai, A. Kostov, and W. W. Armstrong, "Sensory nerve recording for closed-loop control to restore motor functions," *IEEE Trans. Biomed. Eng.*, vol. 40, no. 10, pp. 1024–1031, Oct. 1993.

[15] M. A. Nicolelis, "Brain-machine interfaces to restore motor function and probe neural circuits," *Nat. Rev. Neurosci.*, vol. 4, pp. 417–422, 2003.

[16] D. M. Taylor, S. I. Tillery, and A. B. Schwartz, "Direct cortical control of 3D neuroprosthetic devices," *Science*, vol. 296, pp. 1829–1832, 2002.

[17] R. T. Lauer, P. H. Peckham, and K. L. Kilgore, "EEG-based control of a hand grasp neuroprosthesis," *NeuroReport*, vol. 10, pp. 1767–1771, 1999.

[18] G. E. Loeb and R. A. Peck, "Cuff electrodes for chronic stimulation and recording of peripheral nerve activity," *J. Neurosci. Methods*, vol. 64, pp. 95–103, 1996.

[19] R. B. Stein, T. R. Nichols, J. Jhamandas, L. Davis, and D. Charles, "Stable long-term recordings from cat peripheral nerves," *Brain Res.*, vol. 128, pp. 21–38, 1977.

[20] M. Sahin, D. M. Durand, and M. A. Haxhiu, "Chronic recordings of hypoglossal nerve activity in a dog model of upper airway obstruction," *J. Appl. Physiol.*, vol. 87, pp. 2197–2206, 1999.

[21] W. F. Agnew, D. B. McCreery, T. G. Yuen, and L. A. Bullara, "Histologic and physiologic evaluation of electrically stimulated peripheral nerve: considerations for the selection of parameters," *Ann. Biomed. Eng.*, vol. 17, pp. 39–60, 1989.

[22] G. G. Naples, J. T. Mortimer, A. Scheiner, and J. D. Sweeney, "A spiral nerve cuff electrode for peripheral nerve stimulation," *IEEE Trans. Biomed. Eng.*, vol. 35, no. 11, pp. 905–916, Nov. 1988.

[23] J. Rozman, B. Zorko, and M. Bunc, "Selective recording of electroneurograms from the sciatic nerve of a dog with multi-electrode spiral cuffs," *Jpn. J. Physiol.*, vol. 50, pp. 509–514, 2000.

[24] M. K. Haugland, J. A. Hoffer, and T. Sinkjaer, "Skin contact force information in sensory nerve signals recorded by implanted cuff electrodes," *IEEE Trans. Rehabil. Eng.*, vol. 2, no. 1, pp. 18–25, Mar. 1994.

[25] D. J. Tyler and D. M. Durand, "Functionally selective peripheral nerve stimulation with a flat interface nerve electrode," *IEEE Trans. Neural Syst. Rehabil. Eng.*, vol. 10, no. 4, pp. 294–303, Dec. 2002.
[26] J. Perez-Orive and D. M. Durand, "Modeling study of peripheral nerve recording selectivity," *IEEE Trans. Rehabil. Eng.*, vol. 8, no. 3, pp. 320–329, Sep. 2000.
[27] P. B. Yoo and D. M. Durand, "Selective fascicular recording of the hypoglossal nerve using a multi-contact nerve cuff electrode," presented at the *25th Ann. Int. Conf. IEEE/EMBS*, Cancun, Mexico, 2003.
[28] M. L. Hines and N. T. Carnevale, "The NEURON simulation environment," *Neural Comput.*, vol. 9, pp. 1179–1209, 1997.
[29] J. D. Sweeney, J. T. Mortimer, and D. M. Durand, "Modeling of mamillian myelinated nerve for functional neuromuscular stimulation," in *Proc. 9th Annu. IEEE/EMBS Int. Conf.*, 1987, pp. 1577–1578.
[30] J. B. Hursh, "Conduction velocity and diameter of nerve fibers," *Am. J. Physiol.*, vol. 127, pp. 131–139, 1939.
[31] R. B. Stein, D. Charles, L. Davis, J. Jhamandas, A. Mannard, and T. R. Nichols, "Principles underlying new methods for chronic neural recording," *Can. J. Neurol. Sci.*, vol. 2, pp. 235–244, 1975.
[32] B. Upshaw and T. Sinkjaer, "Digital signal processing algorithms for the detection of afferent nerve activity recorded from cuff electrodes," *IEEE Trans. Rehabil. Eng.*, vol. 6, no. 2, pp. 172–181, Jun. 1998.
[33] W. B. Marks and G. E. Loeb, "Action currents, internodal potentials, and extracellular records of myelinated mammalian nerve fibers derived from node potentials," *Biophys. J.*, vol. 16, pp. 655–668, 1976.
[34] Y. Chen, P. R. Christensen, K. D. Strange, and J. A. Hoffer, "Multi-channel recordings from peripheral nerves: 2. Measurement of selectivity," presented at the *2nd Annu. IFESS Conf. Neural Prosthesis*, Burnaby, Canada, 1997.
[35] S. E. Mackinnon and A. L. Dellon, "Fascicular patterns of the hypoglossal nerve," *J. Reconstr. Microsurg.*, vol. 11, pp. 195–198, 1995.
[36] M. Sahin, D. M. Durand, and M. A. Haxhiu, "Closed-loop stimulation of hypoglossal nerve in a dog model of upper airway obstruction," *IEEE Trans. Biomed. Eng.*, vol. 47, no. 7, pp. 919–925, Jul. 2000.
[37] A. Branner and R. A. Normann, "A multielectrode array for intrafascicular recording and stimulation in sciatic nerve of cats," *Brain Res. Bull.*, vol. 51, pp. 293–306, 2000.
[38] K. Yoshida and K. Horch, "Closed-loop control of ankle position using muscle afferent feedback with functional neuromuscular stimulation," *IEEE Trans. Biomed. Eng.*, vol. 43, no. 2, pp. 167–176, Feb. 1996.
[39] G. Lundborg and L. B. Dahlin, "Anatomy, function and pathophysiology of peripheral nerves and nerve compression," *Hand Clin.*, vol. 12, no. 2, pp. 185–193, 1996.
[40] S. E. Mackinnon, A. L. Dellon, A. R. Hudson, and D. A. Hunter, "Histopathology of compression of the superficial radial nerve in the forearm," *J. Hand Surg. [Am.]*, vol. 11, pp. 206–210, 1986.
[41] D. J. Tyler and D. M. Durand, "Chronic response of the rat sciatic nerve to the flat interface nerve electrode," *Ann. Biomed. Eng.*, vol. 31, pp. 633–642, 2003.
[42] A. Q. Choi, J. K. Cavanaugh, and D. M. Durand, "Selectivity of multiple-contact nerve cuff electrodes: a simulation analysis," *IEEE Trans. Biomed. Eng.*, vol. 48, no. 2, pp. 165–172, Feb. 2001.
[43] L. A. Geddes and L. E. Baker, "The specific resistance of biological material—a compendium of data for the biomedical engineer and physiologist," *Med. Biol. Eng.*, vol. 5, pp. 271–293, 1967.
[44] P. Koole, J. Holsheimer, J. J. Struijk, and A. J. Verloop, "Recruitment characteristics of nerve fascicles stimulated by a multigroove electrode," *IEEE Trans. Rehabil. Eng.*, vol. 5, no. 1, pp. 40–50, Mar. 1997.

Paul B. Yoo (S'02–M'04) was born in Seoul, South Korea, in 1971. He received the B.A.Sc. degree in engineering science (biomedical engineering option) from the University of Toronto, Toronto, ON, Canada, in 1995. He received the M.S. degree in biomedical engineering from the University of Southern California, Los Angeles, in 1998 and the Ph.D. degree in biomedical engineering from Case Western Reserve University, Cleveland, OH, in 2004.

He is currently a Postdoctoral Research Associate with the Department of Biomedical Engineering, Duke University, Durham, NC. His research interests include neural prostheses, computational neuroscience, neurophysiology of biological systems, and medical imaging.

Dominique M. Durand (M'91) was born in Monbazillac, France, in 1951. He received the engineering degree from Ecole Nationale Superieure d'Electronique, Hydrolique, Informatique et Automatique de Toulouse, France, in 1973. In 1974, he received the M.S. degree in biomedical engineering from Case Western Reserve University, Cleveland, OH., worked several years at the Addiction Research Foundation of Toronto, Toronto, ON, Canada, and in 1982 received the Ph.D. degree in electrical engineering from the University of Toronto, the Institute of Biomedical Engineering.

He his currently Professor in the Departments of Biomedical Engineering and Neurosciences and Director of the Neural Engineering Center at Case Western Reserve University. His research interests are in neural engineering and include computational neuroscience, neurophysiology and control of epilepsy, nonlinear dynamics of neural systems, neural prostheses and applied magnetic and electrical field interactions with neural tissue.

Dr. Durand received a National Science Foundation (NSF) Young Investigator Presidential Award as well as undergraduate and graduate teaching awards. He is a Fellow of the American Institute for Medical and Biomedical Engineering. He is the Editor of the *Journal of Neural Engineering*.